Chinese Chemical Letters 35 (2024) 109234

Contents lists available at ScienceDirect

Chinese Chemical Letters

journal homepage: www.elsevier.com/locate/cclet

Engineering particles towards 3D supraballs-based passive cooling *via* grafting CDs onto colloidal photonic crystals

Jie Wu, Xiaoqing Yu*, Guoxing Li*, Su Chen*

State Key Laboratory of Materials-Oriented Chemical Engineering, College of Chemical Engineering, Nanjing Tech University, Nanjing 210009, China

ARTICLE INFO

Article history:
Received 4 August 2023
Revised 17 October 2023
Accepted 22 October 2023
Available online 24 October 2023

Keywords:
Particle engineering
Carbon dots
Colloidal photonic crystals
Passive cooling
Digital coding

ABSTRACT

Particle engineering has opened the floodgates to material science in both fundamental and application field. However, covalent interactions have not yet been adequately designed in the particle engineering for functional colloidal photonic crystals (CPCs). Herein, we achieved covalent coupling between carboxyl-rich poly(styrene-acrylic acid) (P(St-AA)) monodispersed colloidal particles and amine-rich carbon dots (CDs) based on an feasible and universal particle engineering strategy. The designed CDs-grafted P(St-AA) monodispersed colloidal particles initiate a hydrogen bond-driven assembly mode and ensure the construction of large-scale crack-free CPCs. Moreover, the CDs equipped with selective broad-band absorption capacity could improve the saturation of structural colors for high-visibility CPCs. Furthermore, an injectable photonic hydrogel (IPH) is developed to design CPC supraball hydrogel *via* integrating the CDs-grafted P(St-AA) CPC supraballs with supramolecular hydrogel. Combining superior flexibility, sufficient self-healing capacity of supramolecular hydrogel with visual optical information of our CPC supraballs, a cyclically reversible coding and decoding system was developed. Meanwhile, we firstly demonstrated the novel strategy of 3D supraballs-based passive cooling. The designed 3D CPC supraball hydrogel presents nearly full observation angle reflections behavior and excellent water evaporation capacity and achieves 3.6 °C temperature drops, showing the application advantages in 3D thermal management. This work not only provides a new insight for manipulating optical properties of CPCs, but also demonstrates an easy-to-perform platform, as well as indicates the direction for the promising application of CPCs.

Particle engineering, aimed at desired synthesis, functional modification and structural design of nano/micro particles, has been aroused a growing exploration in fundamental and applied science [1–3]. Particle engineering designs have been widely applied in the construction of functional nanomaterials such as optical and electric, especially in regulating the assembly structure, enriching the photoelectric function [4]. Diversiform approaches have been proposed in particle engineering, including ligand-coated strategy [5], doping modification [6], and even coupling technique [7]. Obviously, strong covalent force, which can establish robust chemical interaction between nano/micro particles, is high concern in particle engineering [8,9]. For instance, Dey *et al.* demonstrated a highly robust three-dimensional (3D) nanoparticle supercrystals (NPSCs) driven by covalent bonding interactions. These covalently bonded NPSCs were outstanding in solvent and high-temperature stability [10]. Liu *et al.* combined covalent conjugation strategies and neural regeneration technique, suggesting the great potential of the covalent interactions between cells and biomaterials in tissue regeneration [11]. In addition, covalent interactions are essential to ensure the application performance of functional particles, and efficiently avert the performance attenuation ascribed by functional group stripping on particle surface. In contrast, it is hard to achieve for common weak intermolecular forces, such as van der Waals forces and hydrogen bonding interactions [12,13]. However, covalent interactions have not yet been adequately designed in the particle engineering for the formation of functional monodispersed particles. Thus, the high-efficient and easy-to-perform covalent coupling route towards monodispersed particles remains highly desired.

Colloidal photonic crystals (CPCs) with distinct optical properties, which are derived from the assembly of monodispersed colloidal particles, have been broadly applied in optical displays, anti-counterfeiting encryption, and sensing detection [14–17]. Especially, particle engineering of monodispersed colloidal particles originated from the covalent interactions could exert positive effects in improving structure and performance of CPCs. In this aspect, Chen [18] *et al.* obtained wettability-encoded CPC patterns based on the clickable reaction of alkyl-modified sub-micrometer

* Corresponding authors.
E-mail addresses: xiaoqingyu2208@163.com (X. Yu), xing1065172121@163.com (G. Li), chensu@njtech.edu.cn (S. Chen).

https://doi.org/10.1016/j.cclet.2023.109234
1001-8417/

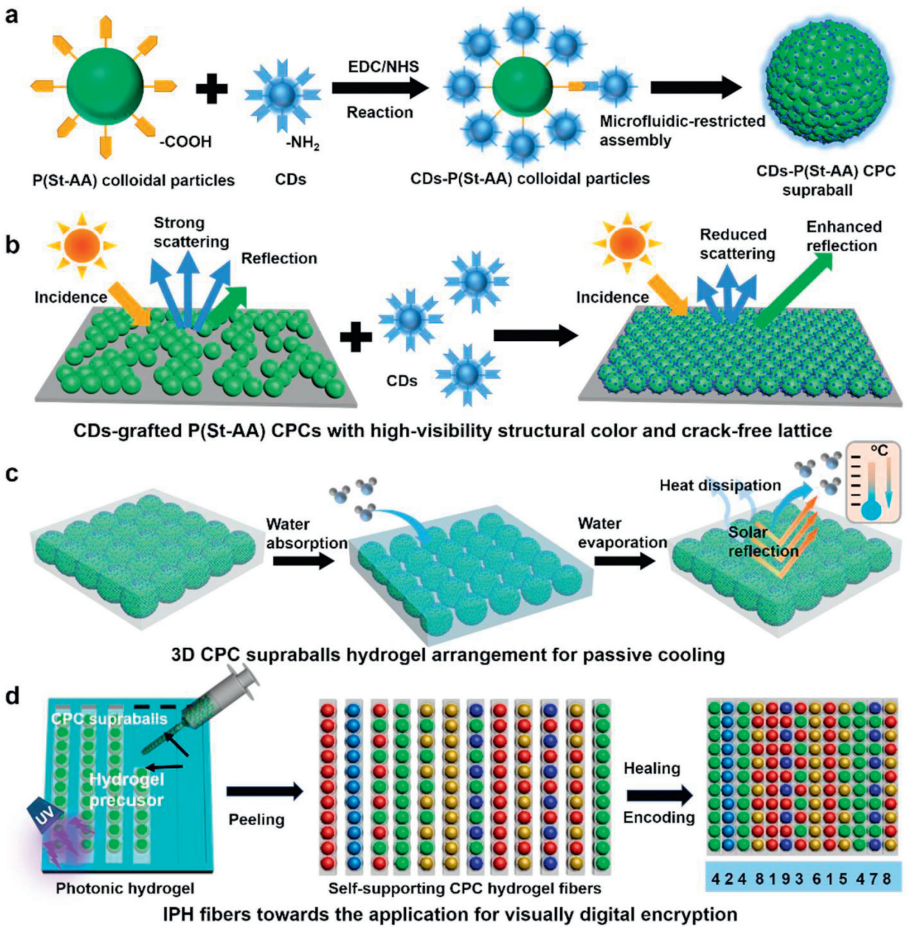

Fig. 1. (a) Schematic illustration of the covalent grafting of amine-rich CDs on monodispersed P(St-AA) colloidal particles. (b) Explanation of the regulation mechanism in structure and optical performance of the CDs-grafted CPCs. (c) Design of 3D CPC supraballs hydrogel arrangement for passive cooling. (d) Description of the fabrication of CPC supraballs hydrogel fibers using a developed IPH system and their application for visually digital coding.

silica particles. Zhang *et al.* [19] prepared Methyl viologen (MV) loaded SiO_2 particles by silane chemistry, and the assembled CPCs features highly saturated and tunable structural colors. Recently, our group firstly ensured the *in-situ* covalent coupling between sub-micro SiO_2 monodispersed colloidal particle and nano-scale carbon dots (CDs) for fluorescent CPCs. The bi-optical responsiveness of the fluorescent CPCs presents significant application advantages towards veterinary drug detection [20]. And thus, the particle engineering is vital for facilitating the progress of the functional and high-quality CPCs. More promisingly, the passive cooling capacity of CPCs conforms to the social trends of energy saving and carbon reduction, would also set off a new wave of applied research [21,22]. The particle engineering would bound to create a powerful approach to the design of photothermal properties of CPCs.

Herein, we achieved covalent coupling between poly(styrene-acrylic acid) (P(St-AA)) monodispersed colloidal particles and CDs *via* a feasible and universal particle engineering strategy. The synthesized CDs-grafted P(St-AA) monodispersed colloidal particles ensure the construction of robust and high-performance CPCs, and greatly expand the application prospect of CPCs in digital coding and passive cooling. This work demonstrates the following distinct strengths: (1) We synthesized CDs-grafted P(St-AA) monodispersed colloidal particles *via* particle engineering, where strong covalent interaction generates from the amination reaction between amine-rich CDs and carboxyl-rich P(St-AA) colloidal particles (Fig. 1a). The CDs-grafted P(St-AA) monodispersed colloidal particles with desired monodispersity (PDI < 0.05) and stability could be employed as the desirable building block of CPCs. (2) Hydrogen bond-driven assembly mechanism is proved based on the CDs-grafted P(St-AA) monodispersed colloidal particles, ensuring large-scale crack-free lattice structure. The morphology and chemical structure of CDs can be well adjusted and designed at the nanoscale (<10 nm), and thus the nanoscale CDs could be firmly anchored on the surface of colloidal particles based on particle engineering. The obtained CDs-grafted P(St-AA) monodispersed colloidal particles provide enhanced hydrogen bond-driven force towards near-periodic lattice structure. Meanwhile, the CDs could act as a light-scattering absorber to uniformly absorb the strong incoherent scattering light, achieving the optimization of the saturation of structural colors for high-visibility CPCs (Fig. 1b). (3) We proposed a novel 3D supraballs-based passive cooling method. The designed 3D CPC supraballs hydrogel establishes nearly full observation angle reflections to effectively shield the solar radiation, while the water evaporation in the 3D hydrogel network accelerates heat dissipation. Significantly, 3.6 °C temperature drops of the 3D CPC supraballs hydrogel successfully achieves the purpose of 3D thermal management (Fig. 1c). (4) Meanwhile, the visual optical information, superior flexibility and sufficient self-healing capacity of the CPC supraballs hydrogel fibers ensure a cyclically reversible coding and decoding of visual recognition system (Fig. 1d). We therefore believe that this work will provide reliable reference for the design of functional and high-quality CPCs, and lay a meaningful foundation for further applications of CPCs.

Aimed at regulating the structure and optical properties of CPCs, we designed CDs-grafted P(St-AA) monodispersed colloidal

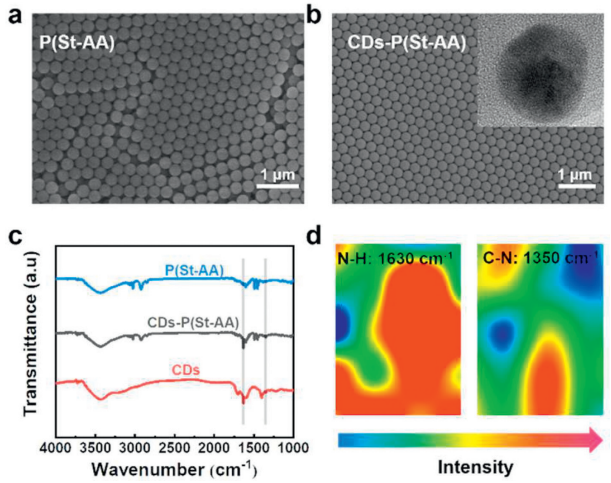

Fig. 2. (a) SEM image of the pure P(St-AA) CPCs. (b) SEM image of CDs-grafted P(St-AA) CPCs. Inset: crystal lattices of the CDs. (c) FT-IR spectra of the pure P(St-AA) CPCs (blue), CDs (red), and CDs-grafted P(St-AA) CPCs (gray). (d) Micro-IR images corresponding to N–H, C–N characteristic absorption peaks of the CDs-grafted P(St-AA) CPCs.

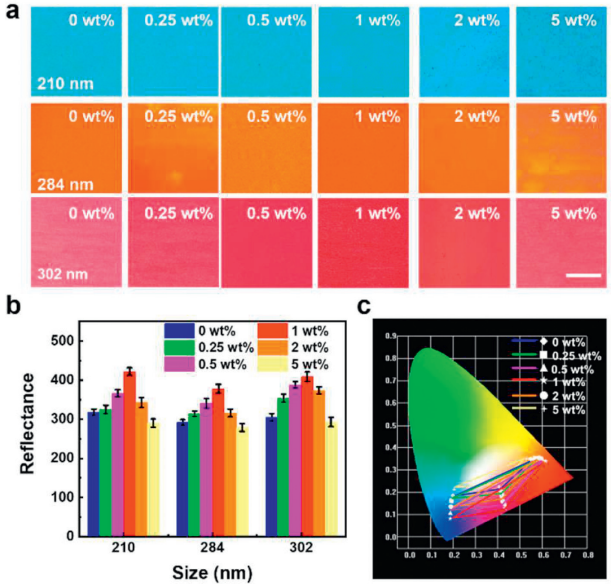

Fig. 3. (a) Optical photographs, (b) intensity of reflection peaks and (c) CIE chromaticity plots of structural color films constructed by CDs-grafted P(St-AA) monodispersed colloidal particles with different CDs concentration (0 wt%, 0.25 wt%, 0.5 wt%, 1 wt%, 2 wt%, and 5 wt%) and different P(St-AA) particles sizes (210, 284, and 302 nm). Scale bar is 1 cm.

particles. To this end, blue amine-rich chiral CDs with an optimal excitation wavelength of 380 nm, optimal photoluminescence (PL) emission wavelength of 450 nm and an absorption peak of 345 nm was developed (Figs. S1 and S2 in Supporting information) [23]. Meanwhile, carboxy-rich P(St-AA) colloidal particles were adopted (Fig. S3 in Supporting information). As shown in Fig. S4 (Supporting information), the resultant P(St-AA) colloidal particles possess high monodispersity (polydispersion index (PDI) < 0.05) with an average particle size of 284 nm. In an amidation reaction, the robust covalent interaction was built between the carboxyl group of P(St-AA) colloidal particles and the amino group of CDs, and the CDs-grafted P(St-AA) colloidal particles were obtained. The size of the CDs-grafted P(St-AA) colloidal particles is 288 nm, which proved that the impact on particle size is negligible during the grafting process. Meanwhile, the PDI of the CDs-grafted P(St-AA) colloidal particles is below 0.05, meaning the excellent monodispersity for generating high-quality CPCs (Fig. S5 in Supporting information).

Scanning electron microscope (SEM) images were taken aimed to evaluate the differences in morphology and distribution of P(St-AA) colloidal particles before and after CDs grafting. Two kinds of circumstances here under, the pure P(St-AA) colloidal particles are regularly spherical in morphology and uniform in size and distribution, while the assembly structure of these particles is relatively disorderly (Fig. 2a). After grafting CDs, the size of the CDs-grafted P(St-AA) colloidal particles increased slightly and the arrangement is more compact (Fig. 2b). Thus, the CDs could effectively promote the assembly of colloidal particles and form a regular hexagonal close-packed lattice. The inset of Fig. 2b points out the lattice structure of CDs (0.28 nm lattice spacing). To some extent, these results reveal the successful synthesis of the CDs-grafted P(St-AA) colloidal particles. We further verified the chemical composition of the pure CDs, pure P(St-AA) and the CDs-grafted P(St-AA) colloidal particles by Fourier-transform infrared (FT-IR) spectroscopy (Fig. 2c). For pure CDs (red curve), the absorption peaks appear at 3430, 1630 and 1350 cm^{-1}, corresponding to characteristic groups of amines, respectively, suggesting the abundant amino group on the CDs surface [24]. Compared to the pure P(St-AA) colloidal particles, the FT-IR curve of CDs-grafted P(St-AA) (gray curve) appears two new absorption peaks at 1630 and 1350 cm^{-1}, which belong to the characteristic peaks of N–H and C–N in CDs, confirming the grafting of CDs onto the P(St-AA) colloidal particles. Furthermore, the micro-IR images of the CDs-grafted P(St-AA) colloidal particles present the N–H and C–N groups with high intensity, which further confirming the formation of amide bond (Fig. 2d). The crystalline structure of the pure P(St-AA) and CDs-grafted P(St-AA) colloidal particle is recorded by X-ray diffraction (XRD) (Fig. S6 in Supporting information). Both pure P(St-AA) colloidal particles ($2\theta = 19°$) and CDs-grafted P(St-AA) colloidal particles ($2\theta = 20°$) show the almost similar wide diffraction peak, indicating their amorphous structure. Whereas, due to the introduction of highly disordered CDs, the characteristic diffraction peak of the CDs-grafted P(St-AA) colloidal particles shifts slightly to the right [25]. These above characterizations successfully confirmed the grafting of CDs on the P(St-AA) colloidal particles surface based on the proposed particle engineering strategy, and clearly indicated the robust covalent interaction.

In addition, the optical property of the CDs-grafted P(St-AA) CPC is probed deeply. Fig. 3a presents a series of CDs-grafted P(St-AA) CPC films with different reflections, which were obtained *via* varying the CDs concentration and the particle size of P(St-AA) colloidal particle. Obviously, the effect of incorporation CDs onto P(St-AA) colloidal particles on the particle size and PDI is fully negligible (Fig. S7 in Supporting information). Therefore, blue, orange, and red structural colors films were derived from colloidal particles of 210, 284 and 302 nm, respectively. In the case of the pure P(St-AA) CPCs, the structural color is relative dim due to negative incoherent light scattering [26]. Whereas, the CPC films made of CDs-grafted P(St-AA) colloidal particles show the enhanced brightness and saturation, which could be explained by the fact of the broadband absorption ability of CDs in the visible region, eliminating incoherent scattering and regulating the Bragg diffraction of the CPCs [27–30]. Obviously, the high-intensity, broad background signal of CPCs was reduced by the CDs-grafted P(St-AA) colloidal particles [31]. The reflection spectra of each of the structural color films were characterized (Fig. 3b, Figs. S8 and S9 in Supporting information) to explore the difference in optical properties. The reflection intensity of CPC film was gradually increased with the CDs concentration (from 0 wt% to 1 wt%). Whereas, the reflection intensity begins to recede as the excessive incorporation of CDs (with

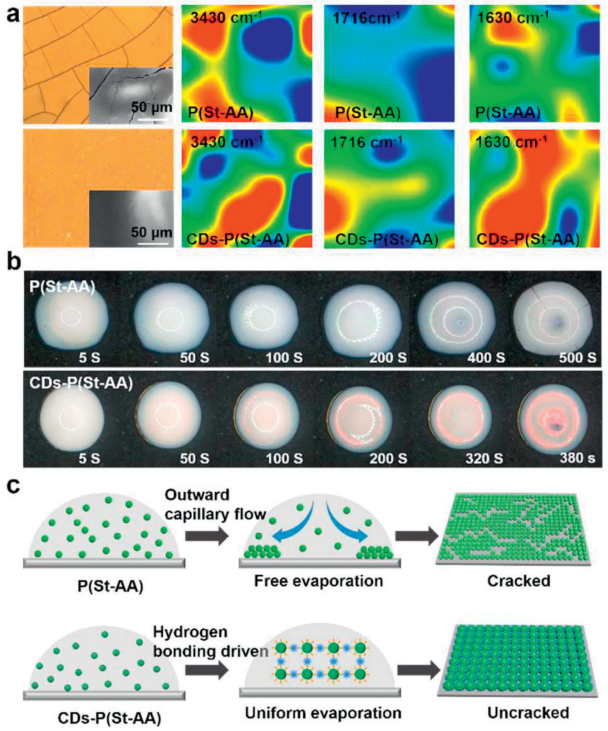

Fig. 4. (a) Optical micrographs of P(St-AA), CDs-grafted P(St-AA) CPC film with the structural color of yellow and IR images of characteristic peaks at 3430, 1716 and 1630 cm^{-1}. Scale bar: 50 μm. (b) Optical images of the assembly process of the pure P(St-AA) colloidal particles (upper) and CDs-grafted P(St-AA) colloidal particles (lower) with same solid content (25 wt%) and similar particle sizes (302 nm) on hydrophilic substrate. (c) Schematic illustration of the evaporation induced self-assembly process of pure P(St-AA) and CDs-grafted P(St-AA) colloidal particles.

CDs concentrations > 1 wt%) due to raised absorption. In comparison, the reflection spectra of pure CPC show a wide and weak peak on account of the high incoherent scattering. It is worth noting that the grafting of CDs (1 wt% concentration) expands the gamut area and greatly increases the color saturation of CPCs (Fig. 3c). And thus, the CDs concentration was determined as 1 wt% for subsequent experiments. Moreover, these results strongly indicate the regulation of CDs on the optical property of CPCs, facilitating the development of CPCs with high-visibility structural color.

Employing bar-coating method, P(St-AA) and CDs-grafted P(St-AA) CPC film were constructed on glass substrate. It is worth noting that visible cracks scattered on the P(St-AA) CPC film, resulting in its poor structural color. By contrast, after grafting CDs, cracks of CPC film are suppressed. To reveal the cause of crack disappearance, micro-IR images of P(St-AA) and CDs-grafted P(St-AA) CPC films were taken. As shown in Fig. 4a, the absorption peaks at 3430, 1716 and 1630 cm^{-1} of CDs-grafted P(St-AA) CPC films are enhanced, corresponding to -OH, C=O and N–H groups, respectively. It is verified that the enhanced hydrogen bond interaction of CDs-grafted P (St-AA) CPC ensures the orderly assembly of colloidal particles and inhibits cracks and defects [32,33]. Furthermore, we compared the assembly behavior of the CDs-grafted P(St-AA) colloidal particles with the pure P(St-AA) colloidal particles (temperature: 30 °C, humidity: 60%, solid content: 25 wt%). Fig. 4b shows the assembling process of monodispersed colloidal particles on a hydrophilic substrate. In the pure P(St-AA) colloidal particles case, the droplet reached surface dry state after 500 s. Based on the evaporation-induced self-assembly, a ring-like deposit with dim color and severe cracks formed. While the CDs-grafted P(St-AA) colloidal particles demonstrate an assemble time as short as 380 s, which is only about 76% of pure P(St-AA) colloidal particles [20]. The enhanced assembly efficiency and excellent assembly performance are desired in CPC application. Taken the above results into consideration, a hydrogen bond-driven self-assembly mechanism of the CDs-grafted P(St-AA) colloidal particles is shown in Fig. 4c. In the most cases, just like P(St-AA) colloidal droplet, the free evaporation self-assembly process of CPCs could produce outward capillary forces, which can eventually lead to the formation of coffee rings at the edges and the occurrence of obvious cracks [34]. Then, the hydrogen bond-driven force of CDs-grafted P(St-AA) colloidal particles opens a more uniform and efficient assembly mode. Therefore, the assembly efficiency of CPCs is greatly enhanced. In addition, the interaction of particles-medium and particle-particle is also enhanced, and the outward capillary flow is destroyed in the CDs-grafted P(St-AA) colloidal droplets, resulting in the disappearance of cracks [35,36].

Taken application into consideration, we fabricated spherical CPCs in a continuous and controllable manner using a single-emulsion microfluidics chip. The generated water-in-oil colloidal droplets through microfluidics chip were regarded as soft spherical mold, which ensuring the spherical morphology and highly ordered arrangement of the obtained CPC supraballs (Fig. S10 in Supporting information) [37,38]. CPC supraballs with different structural color could be attained *via* regulating the size of building blocks. Dazzling blue, green, orange, and red CPC supraballs were prepared from 210, 244, 284, and 302 nm CDs-grafted P(St-AA) monodispersed colloidal particles, respectively. The superimposed light absorption, enhanced reflection, and reduced incoherent scattering of the CDs-grafted CPC supraballs effectively achieved the bright and saturated colors that are visible to the naked eye (Fig. S11 in Supporting information) [24,39]. As the control, the supraballs built by pure P(St-AA) colloidal particles presented whitish color through the naked eye observation. The accurate discrimination of color of these pure CPC supraballs need to be assisted by reflection spectrum or optical microscope, which restricts the acquisition of optical information for application (Fig. S12 in Supporting information) [26]. These CDs-grafted CPC supraballs maintain highly uniform spherical morphology with sizes of ~500 μm. The microstructure of the as-prepared CDs-grafted CPC supraballs was characterized by SEM (Fig. S13 in Supporting information), showing that the CPC supraballs present regular spherical morphology and assembled by close-packed particles. High-resolution SEM images demonstrated that CDs-grafted P(St-AA) monodispersed colloidal particles crystallized into hexagonal close-packed arrangement throughout the whole of supraball. The as-prepared CPC supraballs still exhibit excellent structural and optical stability after being stored in water for up to 45 days (Fig. S14 in Supporting information). Additionally, the colors of these CPC supraballs are noniridescent, which provide a distinct advantage in wide-angle CPC applications (Fig. S15 in Supporting information) [40].

To account for these, we constructed injectable photonic hydrogel (IPH) employing the microfluidics-based CPC supraballs as coloration materials [41]. As shown in Fig. S16 (Supporting information), the absorption peaks appear at 1723, 1635 and 1451 cm^{-1}, corresponding to C=O, -CO–NH-, C=N groups, indicating the successful synthesis of the P(HPA-*co*-VI)/GelMA hydrogel. Being different from the ordered self-assembly of monodispersed particles, we attempted to disperse the CDs-grafted CPC supraballs into P(HPA-*co*-VI)/GelMA hydrogel precursor to produce an IPH. In this respect, these as-prepared CPC supraballs were supported by the supramolecular hydrogel system. Plentiful hydrogen bonds are formed between the CPC supraballs and the hydrogel network, and thus, enhanced mechanical property was achieved (Figs. S17 and S18 in Supporting information). Furthermore, we learned that hydrogel precursors have different physical morphology at different temperatures. It is obvious that when the temperature is above 25 °C, it shows a flow state. While the temperature is below

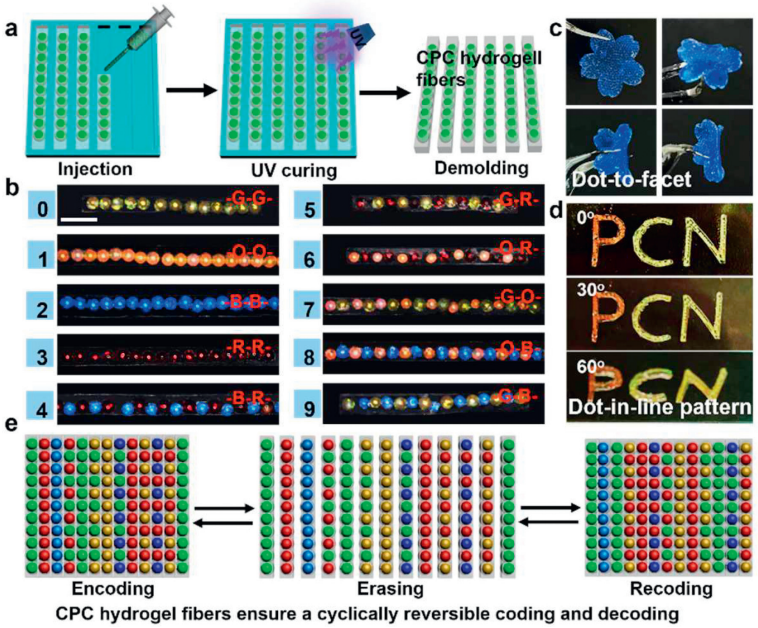

Fig. 5. (a) Cartoon illustration of the preparation of self-supporting CPC supraball hydrogel fibers using an IPH system composed of hydrogel scaffold and CPC supraballs. (b) CPC supraball hydrogel fibers with different structural color represent specific numeric-coded character. Scale bar is 1 mm. (c) Photographs of a sakura-shaped photonic hydrogel pattern in different bending states. (d) Optical images of the dot-in-line structural color pattern originated from the IPH. (e) Schematic illustration of the CPC supraball hydrogel fibers for encoding and recoding.

25 °C, the gelation takes place extremely quickly. Meanwhile, taking advantages of the UV-induced polymerization capacity, a fixed structural photonic hydrogel was achieved by photopolymerization under 365 nm UV light.

This strategy provides a novel guideline for colorant structure by combination of high-visibility CPC supraballs with hydrogel precursor. At this point, we developed dot-in-line CPC supraball hydrogel fibers based on the IPH and microfluidics-constrained assembly strategy. Typically, the IPH was programmed pumped into a bar mold (20 mm × 1 mm) through a round glass capillary with an 800 μm tapered orifice. Based on the microfluidics-constrained assembly, CPC supraballs are arranged into a line in the mold. The packed CPC supraballs could be rapidly fixed (below 25 °C) in the hydrogel precursor due to the temperature-stimulated phase transition behavior of GelMA. Meanwhile, a robust self-supporting CPC supraball hydrogel fiber was easily peeled from mold after UV photopolymerization (Fig. 5a). As shown in Fig. 5b, homogeneous structural color hydrogel fibers were obtained using a single channel. The homogeneous fibers were composed of CPC supraballs with the same reflected wavelength and displayed uniform structural color. Analogously, a Y-channel was designed to produce CPC supraball hydrogel fibers that could appear alternating colors. Consequently, various of CPC supraball hydrogel fibers with different color arrangements were achieved, such as orange-orange (-O-O-), blue-blue (-B-B-) homogeneous CPC supraball hydrogel fibers and orange-blue (-O-B-), and blue-red (-B-R-) heterogeneous CPC supraball hydrogel fibers [42]. Intriguingly, we further designed a sakura-shaped dot-to-facet pattern that could be arbitrarily bended and restored, showing superior flexibility (Fig. 5c) [43]. Besides, dot-in-line structural color patterns could be fabricated with the assistant of tailor-made mold. The "PCN" pattern consisting of linear CPC supraballs keeping their non-iridescent optical property (Fig. 5d). This technique is easy processing, and it is sufficient to achieve CPC supraball hydrogel fibers with arbitrary length and structural color sequence. Meanwhile, structural color patterns could be reliably customized.

The as-designed CPC supraball hydrogel fibers demonstrated specific angle-independent structural color, stability, programmability and efficient readability. Given these excellent properties, we extended this CPC supraball hydrogel fibers to establish a coding-decoding system. Herein, CPC supraball hydrogel fibers with same structural color are employed to represent a specific numeric-coded character, such as green-green (-G-G-) CPC supraball hydrogel fibers represent the number 0, -O-O- CPC supraball hydrogel fibers indicate as the number 1, and -G-B- CPC supraball hydrogel express as the number 9 (Fig. 5b). Furthermore, these individual CPC supraball hydrogel fibers were assembled to line-to-plane hydrogel fiber sequence exploiting the self-healing property. Similar to previously reported self-healing gels [44], and as the Micro-IR image showed in Fig. S19a (Supporting information), both hydroxyl (3440 cm^{-1}) and carboxylic (1737 cm^{-1}) groups at the cut edge of CPC supraball hydrogel fibers have larger red area with relatively high intensity of characteristic peaks. Subsequently, the red area of these characteristic groups gradually weakens, corresponding the new occurrence of hydrogen bonding with relatively uniform green, suggesting the establishment of hydrogen bond interactions between hydroxyl group and carboxyl group (Fig. S19b in Supporting information). Therefore, the self-healing properties of the CPC supraball hydrogel fibers could contribute to the recombination of intermolecular hydrogen bonding (Figs. S19b and S20 in Supporting information) [45,46]. Thus, the fiber sequence could be regarded as a numeric-coded character set to realize the coding of numeral information. It is worth mentioning that such line-to-plane assembly process was reversible, that is, the assembled CPC supraball hydrogel fiber sequence could be simply separated into individual fibers to erase the character set information. And these separated individual fibers can re-emerge as a character for number recoding (Fig. 5e). Fig. S21 (Supporting information) reveals the fiber sequence composed of the self-supporting CPC supraball hydrogel fibers, all of these fibers display saturated and bright structural color that is sufficient to ensure accurate reading of optical information *via* naked eyes. Comparing the CPC supraball hydrogel fiber sequence to its digital coding table, we can quickly decode the optical information of CPCs and obtain the numeric-coded character set (88259186240362) by visual recognition. Meanwhile, the gel fiber sequence could provide another

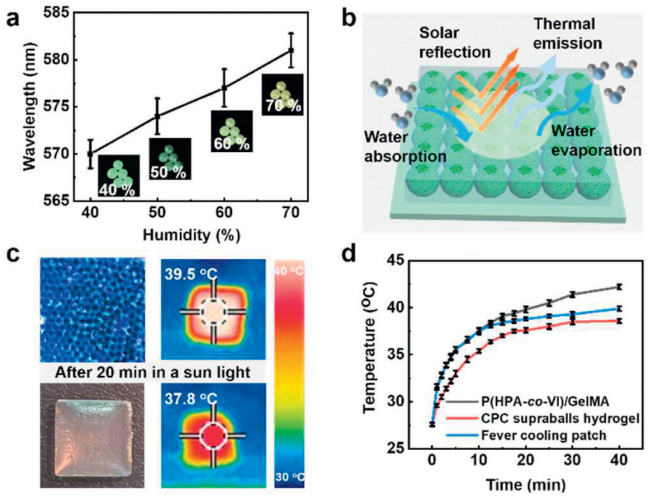

Fig. 6. (a) Optical images and reflection peaks of the CPC supraballs response to different humidity (from 40%–70%). (b) Schematic of near full angle reflection cooler prepared by 3D CPC supraball hydrogel. (c) Optical images and infrared thermal images of the P(HPA-*co*-VI)/GelMA and CPC supraballs hydrogel after 20 min solar irradiation. (d) Temperature-time curves of internal temperature of commercial fever cooling patch, P(HPA-*co*-VI)/GelMA and CPC supraballs hydrogel.

character set of 86829120542638 by reversible recoding. The connection between fibers is strong suffice to be lifted, and the CPC supraball hydrogel fiber sequence could be hanged in the air for a long time (Fig. S22a in Supporting information). Moreover, the CPC supraball hydrogel sequence could be attached on different substrates (glass, paper), providing a wide range of application environments (Fig. S22b in Supporting information).

The highly selective reflection capacity of CPCs could effectively reflect heat back into the surrounding environment for passive cooling [47,48]. Therefore, in another experiment, we were focused on exploring the cooling performance of the 3D CPC supraballs hydrogel. Meanwhile, the water-absorbing properties of hydrogel can absorb water from the air for evaporative cooling [49]. Therefore, taken the synergistic effect of reflective cooling and evaporative cooling into consideration, the 3D CPC supraballs hydrogel was applied for 3D thermal management. As shown in Fig. 6a, the CDs-grafted CPC supraballs display excellent humidity response ability. As the ambient humidity increases from 40% to 70%, the color of the CDs-grafted CPC supraballs gradually changes from the original bright green to yellow, accompanied by the redshift of the reflection peak (570 nm to 581 nm) [50]. Currently, faced with the growing global warming and energy consumption issues, passive cooling researches are on the rise. In this regard, the 3D CPC supraballs hydrogel was designed as Bragg reflectors to selectively reflect solar radiation at close to full observation angle. Meanwhile, the water evaporation of the 3D CPC supraballs hydrogel achieves heat dissipation, which is a promising candidate to 3D passive cooling (Fig. 6b). Fig. 6c shows the optical images and infrared thermal images of P(HPA-*co*-VI)/GelMA and CPC supraballs hydrogel, the corresponding surface temperature is 37.8 and 39.5 °C after 20 min under 1000 W/m^2 simulated solar radiation, respectively. The surface temperature of the CPC supraballs hydrogel is slightly higher than that of P(HPA-*co*-VI)/GelMA, which could be attributed to the excellent thermal absorption properties of CDs. In addition, we placed P(HPA-*co*-VI)/GelMA, commercial fever cooling patch, CPC supraballs hydrogel on PMMA substrates and traced their internal temperature (Fig. S23 in Supporting information). After 40 min irradiation (intensity of 1000 W/m^2), the temperature increase occurs on the P(HPA-*co*-VI)/GelMA and commercial fever cooling patch, and eventually settles at 42.2 and 39.9 °C. while the temperature of CPC supraballs hydrogel increased from 27.6 °C to 38.6 °C (Fig. 6d). These results indicate that the excellent properties of nearly full observation angle reflection and evaporative cooling of the designed 3D CPC supraballs hydrogel could provide an effective approach for 3D thermal management.

In summary, we proposed a feasible and universal particle engineering strategy to construct CPC films and supraballs with highly tunable and saturated structural color by covalent coupling the as-prepared P(St-AA) monodispersed colloidal particles with amine-rich CDs. The synthesized CDs-grafted P(St-AA) monodispersed colloidal particles not only demonstrate a hydrogen bond-driven assembly mechanism, but also provide broad-band absorption capacity, ensuring the achievement of large-scale and crack-free CPCs with high-visibility structural color. By integrating the IPH with microfluidics technology, we designed the structural color-encoded CPC supraballs hydrogel. In virtue of superior flexibility, sufficient self-healing capacity, and visual optical information of our CPC supraballs hydrogel fibers, a cyclically reversible coding and decoding visual recognition system was developed. This creates great prospect in the new-generation information encryption and anti-counterfeiting devices. In addition, 3D supraballs-based passive cooling was firstly demonstrated by taking advantage of the nearly full observation angle reflection and excellent water evaporation of the 3D CPC supraballs hydrogel, a maximum temperature drops of 3.6 °C under 1000 W/m^2 solar radiation was attained by the 3D CPC supraballs hydrogel, setting off a great wave of 3D passive cooling. This work provides a feasible and universal strategy for the improvement of the high-quality and high-visibility CPCs, and provides novel insights into microfluidics-based CPC supraballs toward digital coding and passive cooling applications.

Declaration of competing interest

The authors declare that they have no known competing financial interests or personal relationships that could have appeared to influence the work reported in this paper.

Acknowledgments

This work was supported by the National Natural Science Foundation of China (No. 22278225) and Priority Academic Program Development of Jiangsu Higher Education Institutions (PAPD).

Supplementary materials

Supplementary material associated with this article can be found, in the online version, at doi:10.1016/j.cclet.2023.109234.

References

[1] J. Zhou, Z. Lin, M. Penna, et al., Nat. Commun. 11 (2020) 4804.
[2] D. Cun, C. Zhang, H. Bera, M. Yang, Adv. Drug. Deliv. Rev. 174 (2021) 140–167.
[3] D. Wu, J. Zhou, M.N. Creyer, et al., Chem. Soc. Rev. 50 (2021) 4432–4483.
[4] Y. Wang, K. Xia, L. Wang, et al., Small 17 (2021) 2005578.
[5] P. Angelikopoulos, L. Sarkisov, Z. Cournia, P. Gkeka, Nanoscale 9 (2017) 1040–1048.
[6] J.M. Jimenez, G.R. Bourret, T. Berger, K.P. McKenna, J. Am. Chem. Soc. 138 (2016) 15956–15964.
[7] Y. Li, D. Shen, H. Zhang, Z. Liu, Chin. Chem. Lett. 34 (2023) 108048.
[8] Y. Ju, C.J. Kim, F. Caruso, Acc. Chem. Res. 56 (2023) 1826–1837.
[9] X. Zhu, Y. Chen, Y. Hu, et al., Food Hydrocolloid. 111 (2021) 106179.
[10] J. Dey, S.J. Lee, J. Kim, et al., Nano Lett. 21 (2021) 258–264.
[11] W. Liu, B. Xu, S. Zhao, et al., Sci. Adv. 9 (2023) eade8829.
[12] K.T. Mahmudov, M.N. Kopylovich, M.F.C. Guedes da Silva, A.J.L. Pombeiro, Coord. Chem. Rev. 345 (2017) 54–72.
[13] M. Schmudde, C. Grunewald, C. Goroncy, et al., ACS Nano 10 (2016) 3525–3535.
[14] F. Qi, Z. Meng, M. Xue, L. Qiu, Anal. Chim. Acta. 1123 (2020) 91–112.
[15] A.Q. Xie, Q. Li, Y. Xi, L. Zhu, S. Chen, Acc. Mater. Res. 4 (2023) 403–415.
[16] J. Hou, M. Li, Y. Song, Angew. Chem. Int. Ed. 57 (2018) 2544–2553.
[17] J. Li, W. Li, Y. Rao, et al., Chin. Chem. Lett. 32 (2021) 150–153.
[18] J. Chen, P. Liu, X. Du, Z. Xie, Langmuir 34 (2018) 13219–13224.

[19] J. Zhang, Z. Meng, J. Liu, S. Chen, Z. Yu, ACS Appl. Mater. Interfaces 11 (2019) 42629–42634.
[20] X.Q. Yu, Y. Zhang, Y. Qiu, et al., Chem. Eng. J. 465 (2023) 142851.
[21] S. Yu, Q. Zhang, Y. Wang, Y. Lv, R. Ma, Nano. Lett. 22 (2022) 4925–4932.
[22] A.Q. Xie, L.L. Zhu, Y. Liang, et al., Angew. Chem. Int. Ed. 61 (2022) e202208592.
[23] C. Liu, R. Cheng, J. Guo, et al., Chin. Chem. Lett. 33 (2022) 304–307.
[24] G. Li, R. Cheng, H. Cheng, et al., Chem. Eng. J. 405 (2020) 126539.
[25] S.S. Suner, M. Sahiner, R.S. Ayyala, V.R. Bhethanabotla, N. Sahiner, J. Fluoresc. 31 (2021) 1705–1717.
[26] D. Huang, M. Zeng, L. Wang, L. Zhang, Z. Cheng, RSC Adv. 8 (2018) 34839–34847.
[27] M. Kohri, K. Yanagimoto, A. Kawamura, et al., ACS Appl. Mater. Interfaces 10 (2018) 7640–7648.
[28] Y. Zhang, P. Han, H. Zhou, et al., Adv. Funct. Mater. 28 (2018) 1802585.
[29] Y. Sun, S. Liu, L. Sun, et al., Nat. Commun. 11 (2020) 5591.
[30] Q. Chang, Z. Song, C. Xue, N. Li, S. Hu, Mater. Lett. 218 (2018) 221–224.
[31] M. Xiao, Z. Hu, Z. Wang, et al., Sci. Adv. 3 (2017) e170115.
[32] C. Liu, A.Q. Xie, G.X. Li, et al., ACS Appl. Polym. Mater. 3 (2021) 6130–6137.
[33] A.Q. Xie, J. Guo, L. Zhu, S. Chen, Chem. Eng. J. 415 (2021) 128950.
[34] D. Mampallil, H.B. Eral, Adv. Colloid Interf. Sci. 252 (2018) 38–54.
[35] J. Zhang, Z. Zhu, Z. Yu, et al., Mater. Horiz. 6 (2019) 90–96.
[36] J. Shi, L. Yang, C.D. Bain, ACS Appl. Mater. Interfaces 11 (2019) 14275–14285.
[37] L.W. Hao, J.D. Liu, Q. Li, et al., J. Mater. Sci. Technol. 81 (2021) 203–211.
[38] C. Liu, H. Li, R. Cheng, et al., J. Mater. Sci. Technol. 104 (2022) 163–171.
[39] Y.G. Kim, S. Park, Y.H. Choi, S.H. Han, S.H. Kim, ACS Nano 15 (2021) 12438–12448.
[40] G. Peng, Z. Zhu, Y. Tian, et al., J. Mater. Chem. C 6 (2018) 8187–8193.
[41] Z. Zhu, J.D. Liu, C. Liu, et al., Small 16 (2020) 1903939.
[42] Q. Li, Y.W. Zhang, C.F. Wang, D.A. Weitz, S. Chen, Adv. Mater. 30 (2018) 1803475.
[43] J. Zhou, P. Han, M. Liu, et al., Angew. Chem. Int. Ed. 56 (2017) 10462–10466.
[44] Z.L. He, J.D. Liu, J. Hu, et al., J. Mater. Sci. 57 (2022) 12971–12984.
[45] B. Yang, J. Song, Y. Jiang, et al., ACS Appl. Mater. Interfaces 12 (2020) 57782–57797.
[46] R. Yu, M. Li, Z. Li, et al., Adv. Healthc. Mater. 11 (2022) 21027.
[47] M. Chen, D. Pang, J. Mandal, et al., Nano Lett. 21 (2021) 1412–1418.
[48] H. Zhang, K.C.S. Ly, X. Liu, et al., Proc. Natl. Acad. Sci. U. S. A. 26 (2020) 14657–14666.
[49] L. Xu, D.W. Sun, Y. Tian, T. Fan, Z. Zhu, Chem. Eng. J. 457 (2023) 141231.
[50] J. He, X. Shen, H. Li, et al., ACS Appl. Mater. Interfaces 14 (2022) 27251–27261.